Solar Cells

DOI: 10.1002/anie.200906933

Double-Layered Photoanodes from Variable-Size Anatase TiO_2 Nanospindles: A Candidate for High-Efficiency Dye-Sensitized Solar Cells

*Yongcai Qiu, Wei Chen, and Shihe Yang**

We report on the use of TiO_2 nanospindles of different sizes to construct a double-layered photoanode for dye-sensitized solar cells (DSSC). One layer made of larger nanospindles enhances light scattering, and the other consisting of smaller nanospindles increases the roughness factor for efficient dye adsorption. The two-layer structure with variable-size, single-crystalline TiO_2 nanospindles exhibits greater than 8.3% energy conversion efficiency. This was made possible by our successful large-scale synthesis of size-tunable, single-crystalline anatase TiO_2 nanospindles.

Dye-sensitized solar cells have attracted extensive interest as a potential low-cost, clean, and renewable energy source.[1–5] Nanocrystalline TiO_2 and ZnO have been the main photoanode materials for developing high performance DSSCs.[1–13] Efficient light harvesting by taking advantage of the light-scattering effect plays a salient role in enhancing the performance of photovoltaic devices.[14–21]

Although a porous electrode made of anatase TiO_2 nanocrystallites (ca. 20 nm in diameter) with a high internal surface area is essential for loading large amounts of dye molecules,[1] such films usually exhibit high transparency, which results in transmittance of a portion of the visible light. Conventionally, a second layer of anatase particles 200–400 nm in diameter is used to form a light-scattering layer.[22,23] Another key issue pertains to the improvement of charge-collection efficiency by minimizing recombination of photoinduced electrons with I_3^- in the electrolyte. For example, aligned single-crystalline ZnO and TiO_2 nanowires,[6,24] quasi-ordered arrays of TiO_2 nanotubes,[7,8] and core/shell nanostructures[25,26] have been conceived and prepared to tackle this issue. However, the cell performance based on these structures reported to date is still far below those of nanoparticle-based TiO_2 photoanodes due to low specific surface area and/or other limiting factors. In general, high specific surface area, fast electron transport, and pronounced light-scattering effect are indispensable to a high-performance photoanode, but these factors are often incompatible with one another. To accommodate all of these favorable characteristics, we propose a double-layered film structure with two different sizes of TiO_2 nanospindles for DSSC photoanodes. We have succeeded in the synthesis of such nanospindles with diameters tunable from 6 to 45 nm and lengths from 20 to 300 nm. These single-crystalline TiO_2 nanospindles are ideal for constructing mesoscopic photoanode films due to the presence of far fewer surface defects than in disordered nanoparticles. Indeed, DSSCs based on these photoanodes have achieved much improved efficiency compared to cells prepared with standard Degussa P25 TiO_2 photoanodes. Also, the novel double-layered photoanode made from different-sized TiO_2 nanospindles not only provides high specific surface area, but also displays stronger aggregation-induced light scattering in the visible wavelength range compared to those made from P25 TiO_2 nanoparticles.

The nanospindles were prepared by hydrothermal treatment of hydrogen titanate in water and different alcohols (see Experimental Section). The large nanospindles were formed in water/ethanol solution, and the small nanospindles in water/ethylene glycol. As can be seen in Figure S1 (see Supporting Information), the hydrogen titanate starting material was indeed transformed into anatase TiO_2 (JCPDS card no. 21-1272). No other secondary phases were observed. The average crystallite sizes of the as-prepared products were calculated to be around 37 (Figure S1, **a**) and 9 nm (Figure S1, **b**), respectively, by applying the Scherrer equation to the broadened (101) diffraction line.

Scanning electron microscopy (SEM) and transmission electron microscopy (TEM) images (Figure 1) clearly revealed the unique morphologies of the as-synthesized TiO_2 nanospindles and their films. The large TiO_2 spindles have a proclivity to bundling, and the film is apparently formed by close packing of the nanospindle bundles (Figure 1a). The nanospindle bundles are effective light scatterers, and this is the basis for using them to construct light-scattering layers (see below). When dispersed, the large TiO_2 nanospindles exhibit well-defined morphology and a uniform diameter of about 35 nm and length of about 250 nm (Figure 1b). The high-resolution (HR) TEM image in Figure 1c, together with the corresponding selected-area electron diffraction (SAED) pattern in Figure 1d, identifies the orientational relationship between the exposed surfaces near a TiO_2 nanospindle tip. The lattice spacing of 3.5 Å can be ascribed to the (101) planes of anatase TiO_2, which form an angle with the (001) main spindle axis. The well-defined spots of the SAED pattern indicate good crystallinity of the nanospindle and confirm the preferred growth direction along the *c* axis. The tip is thus bounded by two sets of (101) surfaces with lower energy due to adsorption of organic amines.[27,28]

[*] Y. Qiu, Dr. W. Chen, Prof. Dr. S. Yang
Department of Chemistry
Hong Kong University of Science and Technology
Clear Water Bay, Kowloon, Hong Kong (China)
E-mail: chsyang@ust.hk

Supporting information for this article is available on the WWW under http://dx.doi.org/10.1002/anie.200906933.

© 2010 Wiley-VCH Verlag GmbH & Co. KGaA, Weinheim

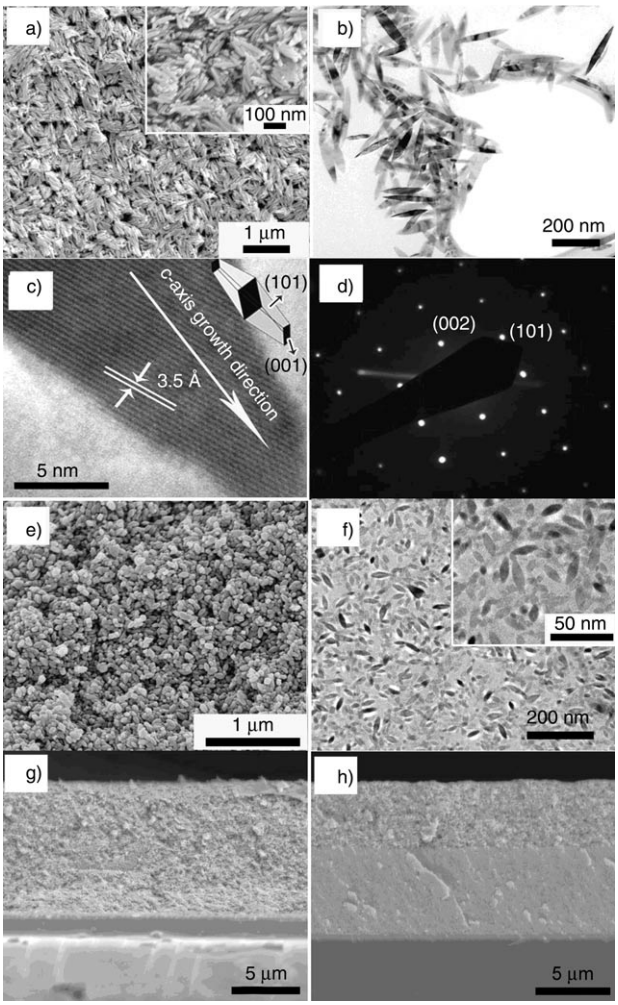

Figure 1. a, b) SEM and TEM images of the as-prepared large TiO_2 nanospindles. c, d) HRTEM image and the corresponding SAED pattern of a typical nanospindle. e, f) SEM and TEM images of the as-prepared small TiO_2 nanospindles. Cross-sectional SEM images for a single mesoscopic TiO_2 layer prepared from large nanospindles (g) and a double-layer structure from large and small nanospindles (h). Inset of a): Enlarged SEM image showing the close packing of large TiO_2 nanospindle bundles. Inset of c): Schematic illustration of the anatase crystal planes of TiO_2 nanospindles. Inset of f): Enlarged TEM image of the as-prepared small TiO_2 nanospindles.

Small TiO_2 nanospindles obtained from a viscous water/ethylene glycol solution are shown in Figure 1e and f. The well-defined shape, size (ca. 8×20 nm), and uniformity of the nanospindles are clearly recognizable. Figure 1g and h show SEM cross-sectional images of a single-layered film (ca. 10.6 μm nanospindles) and a double-layered structure (ca. 6.1 μm nanospindles and ca. 4.7 μm nanospindles) on fluorine-doped tin oxide (FTO) substrates, respectively. For comparison, standard Degussa P25 TiO_2 was also used to prepare a film of the same thickness by the same doctor-blade technique (see film morphology in Figure S2a). The Brunauer–Emmett–Teller (BET) surface areas of these films (Table 1) are 35.1 (large nanospindles, DSC-1), 76.1 (double-layered nanospindles, DSC-2), and 51.2 $m^2 g^{-1}$ (P25, DSC-3), respectively. The surface area of the double-layered

Table 1: Structural and performance characteristics of DSSCs based on photoanodes of DSC-1, DSC-2, and DSC-3.

DSSC	V_{oc} [mV]	J_{sc} [mA cm^{-2}]	*FF* [%]	η [%]	Surface area [m^2 g^{-1}]	Adsorbed dye [×10^{-7} mol cm^{-2}]
DSC-1	755	8.4	67.8	4.30	35.1	0.89
DSC-2	760	16.4	66.8	8.32	76.5	1.66
DSC-3	750	11.6	66.6	5.79	51.2	1.18

SP film is 1.49 times that of the film derived from P25, and clearly benefits from the high surface-to-volume ratio of the small nanospindles. The pore size distributions of the three films determined from their N_2 absorption/desorption isotherms are shown in Figure S3. The P25 film shows a narrow pore size distribution centered at 21.0 nm, which suggests that the irregularly shaped nanoparticles with a mean grain size of about 25 nm are well organized (Figure S2b). While the other two films both display broad pore size distributions (18–80 nm for the single layer of large nanospindles, and 11–70 nm for the double layer of small and large nanospindles), the double-layered film has a narrow pore size distribution around 15.8 nm, which clearly alludes to its main origin from the interstitial voids arising from the close packing of small TiO_2 nanospindles. The narrow average pore size still appears suitable for DSSCs with abundant dye adsorption, efficient electrolyte transport, and hence high performance.

After dye loading, cells with a single layer of large nanospindles (DSC-1), a double layer of small and large nanospindles (DSC-2), and P25 (DSC-3), were subjected to measurements of current–voltage (*J*–*V*) characteristics under illumination of AM 1.5 simulated sunlight with a power density of 100 mW cm^{-2}. Figure 2 shows the *J*–*V* curves of

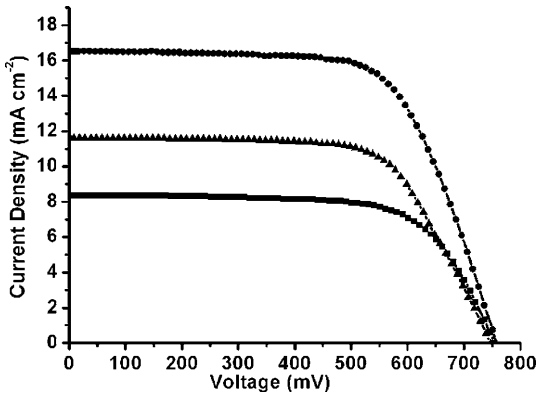

Figure 2. *J*–*V* curves of DSSCs fabricated from the three TiO_2 samples under AM 1.5 G simulated sunlight with a power density of 100 mW cm^{-2}. ■ DSC-1; ● DSC-2; ▲ DSC-3.

these solar cells, and the resultant photovoltaic parameters are summarized in Table 1. The approximately 10.5 μm-thick TiO_2 photoanode made of P25 nanoparticles showed a short-circuit current density (J_{sc}) of 11.6 mA cm^{-2}, open-circuit voltage (V_{oc}) of 750 mV, and fill factor (FF) of 66.6, which lead to an overall energy-conversion efficiency (η) of 5.8%. The performance of DSC-1 derived from a single layer of large

 © 2010 Wiley-VCH Verlag GmbH & Co. KGaA, Weinheim

TiO_2 nanospindles is slightly lower ($\eta = 4.3$) than that of DSC-3 due to decreased dye loading. However, DSC-2 made from a double layer of small and large nanospindles shows superior performance to both DSC-1 and DSC-3. It exhibits higher J_{sc} (16.4 mA cm^{-2}), V_{oc} (760 mV), and FF (66.8%), and thus η reaches up to 8.3%. The enhanced J_{sc} for DSC-2 can be understood as the result of high dye loading in the first layer and enhanced light scattering in the second layer, as well as improved charge collection efficiency due to the use of high-quality single-crystalline nanospindles.

The amounts of N719 dye anchored on these films were investigated by thorough desorption in 1 mM NaOH solution. The dye loading of DSC-2 is 1.8 times higher than that of DSC-1, and 1.4 times that of DSC-3A (see Table 1). The higher dye loading of DSC-2 is ascribed to the larger specific surface area of the film, mainly derived from the first layer due to the small nanospindles.

Photoanode films made from nanoparticles usually exhibit high transparency and negligible light scattering. Enhanced of light scattering of TiO_2 photoanode films is important for improving the light-harvesting efficiency. The diffuse-reflectance spectra of the three TiO_2 films of reflect the differences in light-scattering capability (Figure 3). All

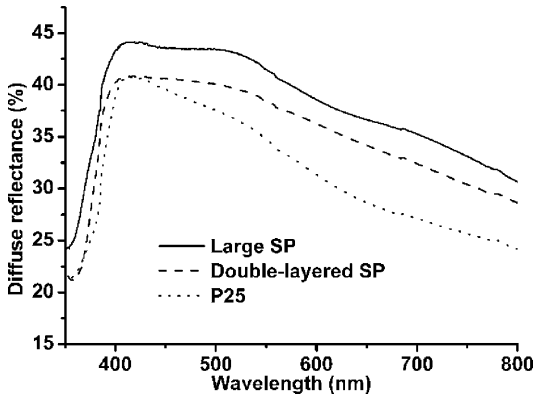

Figure 3. Diffuse-reflectance spectra of the three films of large nanospindles, double-layered SP and P25. —— large SP; ----- double-layered SP; ••••• P25.

three films have high diffuse reflection in the visible range of 400–500 nm, but a distinctly rapid decline in light-scattering capability is observed for P25 film in the wavelength range from 500 to 800 nm. Compared with the P25 film, the other two films, which contain large nanospindles, have better light-scattering properties in the visible and near-infrared regions. The enhanced light scattering is likely due to spontaneous aggregation of nanospindles on evaporation of the solution (see Figure 1a).

Figure 4a shows incident photon to current efficiency (IPCE) spectra for the three DSSCs; DSC-2 has the highest IPCE values over the whole spectral range, mainly due to higher dye loading. The quantum efficiency of the films containing large nanospindles in the longer wavelength region (600–750 nm) is much more prominent than that of the P25 TiO_2 film.[17] It can be ascribed to the enhanced light-scattering effect of these two films, which boosts light

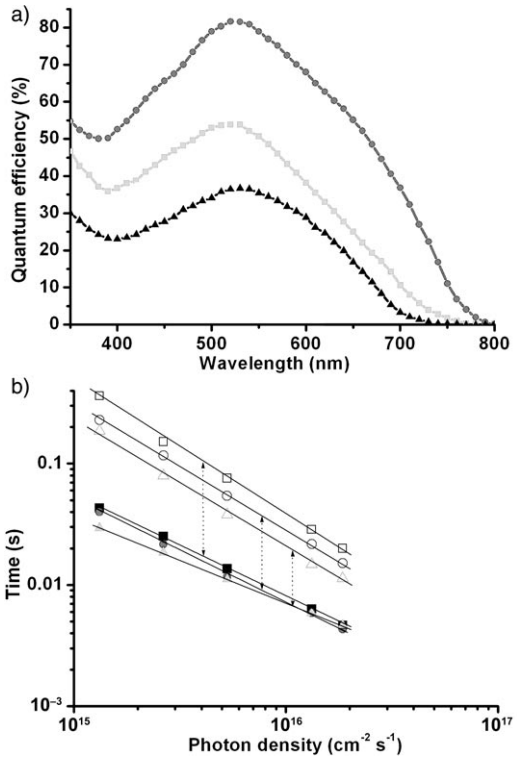

Figure 4. a) IPCE spectra of DSC-1 (large nanospindles), DSC-2 (double-layered nanospindles) and DSC-3 (P25). ▲ DSC-1; ● DSC-2; ■ DSC-3. b) Variation of electron lifetimes and electron transit times for the three DSSCs with the incident light intensity. The straight lines represent power-law fits. Open symbols: Recombination times with I_3^- ions; Filled symbols: electron transit times. ■,□ DSC-1; ●,○ DSC-2; ▲,△ DSC-3.

harvesting in this region, in concurrence with the above diffuse-reflection results.

Intensity-modulated photocurrent spectroscopy (IMPS) and intensity-modulated photovoltage spectroscopy (IMVS) can provide further information on charge collection in DSSCs.[7,8,29–31] Figure 4b plots τ_t and τ_r of photogenerated electrons as a function of the incident photon flux (light intensity, I_0) for the three DSSCs, where τ_t and τ_r are electron transit time across the photoanode films and recombination times of electrons with I_3^- ions in the electrolyte, respectively. Clearly, DSC-1 and DSC-2 show longer lifetimes than DSC-3, which can be explained by the nanospindle films' having fewer surface trapping sites for mediating recombination with I_3^- in the electrolyte. At low light density, electron transport in DSC-2 is slightly faster than in DSC-1, but appreciably slower than in DSC-3, which suggests that electron transport between nanospindles is more difficult than between P25 nanoparticles. Electron transport in DSC-3 became slower than in DSC-1 and DSC-2 at high light density (> 70 W m^{-2}), and this again suggests that more trapping sites are present in film derived from the irregularly shaped and sized P25 TiO_2 nanoparticles. Therefore, for the DSSCs derived from TiO_2 nanospindles, the larger the gap between τ_t and τ_r, the higher the charge-collection efficiency.

Thus, the double-layered film combines the high specific surface area of small nanospindles, which is essential for

 © 2010 Wiley-VCH Verlag GmbH & Co. KGaA, Weinheim

anchoring large amounts of dye to generate high current density, with the enhanced light-scattering capability of spontaneously packed bundles of large nanospindles, which plays an important role the long-wavelength region and results in improved light-harvesting efficiency. In addition, the nanospindle photoanode has fewer traps for mediating recombination with I_3^- in the electrolyte than that made from nanoparticles (see the above IMPS and IMVS measurements). Therefore, the double-layered photoanode has higher charge-collection efficiency than the P25 photoanode.

In conclusion, we have realized a novel double-layered photoanode by using two different sizes of anatase TiO_2 nanospindles, obtained by a facile and scalable process. Such photoanodes not only anchor large amounts of dye molecules but also enhance light-harvesting efficiency through light scattering from the nanospindle aggregates. In addition, the faceted TiO_2 nanospindles are single-crystalline with few surface defects. Hence, the photoanode shows higher charge-collection efficiency than a P25 TiO_2 photoanode. Our preliminary tests have already yielded a rather high energy-conversion efficiency of 8.3% for the double-layered photoanode. We anticipate that a judicious combination of size-tunable, aggregation-prone, single-crystalline TiO_2 nanospindles and double-layered photoanode design will open up an alternative avenue for the development of high-performance DSSCs.

Experimental Section

Synthesis of hydrogen titanate: In a typical synthesis, 0.4 g of TiO_2 (Degussa P25, about 20% rutile and 80% anatase with a particle size of about 20–30 nm) was dispersed in a 20 mL of 10 M aqueous NaOH solution. After stirring for 30 min, the resulting suspension was transferred into a Teflon-lined stainless steel autoclave with a capacity of 100 mL. The autoclave was maintained at 150 °C for 20 h and then allowed to cool to room temperature. The resulting precipitate was stirred in 0.1 M HCl solution until pH 1–2 was reached. The resulting material was then collected by filtration and washed several times with distilled water.

Synthesis of TiO_2 nanospindles of different sizes: The hydrogen titanate was redispersed in water/ethanol (60 mL, 1/1 v/v) or water/ethylene glycol (60 mL, 1/5 v/v) by vigorous stirring of the suspension for 30 min. Then, 2 mL of dimethylamine was added and stirring was continued for 30 min. Then, the mixture was sealed in a Teflon-lined stainless steel autoclave with a capacity of 100 mL and maintained at 180 °C for 10 h, after which the autoclave was allowed to cool to room temperature. The white product of aggregated large spindles was obtained by slow evaporation of the water/ethanol solvents. But to obtain the product of the small spindles, the solvent evaporation was accompanied by repeated addition of water to remove the residual ethylene glycol.

Fabrication and testing of TiO_2 photoanode films: After washing with distilled water several times, the precipitate of small TiO_2 nanospindles was dispersed in 5 mL of water. A drop of Triton X100 was then added into the dispersed solution. A viscous paste was obtained after concentrating the solution by heating. A paste was prepared from large TiO_2 nanospindles by dispersing the powder (0.5 g) and PEG20000 (0.1 g) in water (1 mL) containing acetylacetone and Triton X-100. P25 paste was prepared as reported in the literature.[17,32] Films were fabricated on a conducting substrate (FTO-coated glass, 14 Ω/square, Nippon Sheet Glass, Japan) by doctor blading with adhesive tape (Scotch brand) as frame and spacer. To improve the performance of these DSSCs, prior to coating with the main TiO_2 layer, a thin interfacial TiO_2 blocking layer was deposited onto the well-cleaned FTO glass substrate by immersion in 0.2 M $TiCl_4$ solution for 12 h, followed by heating in air at 500 °C for 0.5 h.[21] After cooling to 80 °C, the TiO_2 films were loaded with dye by immersing them in a 0.5 mM solution of N719 dye (bis-tetrabutylammonium *cis*-bis(isothiocyanato)bis(2,2′-bipyridyl-4,4′-dicarboxylato)ruthenium(II), Suzhou Chemsolarism, China) in acetonitrile/*tert*-butyl alcohol (1/1 v/v) containing 5×10^{-4} M N719 for 24 h. These dye-coated electrodes were assembled into solar cells with Pt-sputtered FTO counterelectrodes and acetonitrile/valeronitrile (85/15 v/v) electrolyte containing 0.6 M 1,2-dimethyl-3-propylimidazolium iodide, 0.03 M I_2, 0.1 M guanidinium thiocyanate, and 0.5 M 4-*tert*-butylpyridine. We determined the amount of adsorbed dye by immersing the films in 1 mM NaOH solution (water/ethanol 1/1 v/v) and monitoring the concentration of desorbed dye by UV/Vis spectroscopy. The light source (Oriel solar simulator, 450 W Xe lamp, AM1.5 global filter) was calibrated to 1 sun (100 mW cm^{-2}) by using an optical power meter (Newport, model 1916-C) equipped with a Newport 818P thermopile detector. *J–V* characteristic curves and intensity-modulated photocurrent/photovoltage spectra (IMPS/IMVS) were measured by the Zahner Zennium C-IMPS system. IPCE was measured on the basis of a Jobin-Yvon Triax 190 monochromator. The photoanode film area for the DSSC performance test was typically 0.25 cm^2.

Characterization: Morphologies of the nanomaterials were directly examined by SEM with a JEOL6700F at an accelerating voltage of 5 kV. TEM observations were carried out on a JEOL 2010F microscope operating at 200 kV. BET surface areas and pore size distributions of the film samples were characterized by using a Coulter SA 3100 surface area analyzer. The samples for BET characterization were obtained by scraping the as-prepared films from the conductive glass substrates. XRD patterns of the film samples on glass slides were obtained with a Philips high-resolution X-ray diffraction system (model PW1825). Diffuse-reflectance spectra were measured on the same film samples on a Perkin-Elmer UV/Vis spectrophotometer (model Lambda 20). The film thickness was determined by a Tencor Alpha-Step 200 surface profiler system.

Received: December 9, 2009
Published online: April 7, 2010

Keywords: hydrothermal synthesis · nanostructures · photophysics · solar cells · titania

[1] B. O'Regan, M. Grätzel, *Nature* **1991**, *353*, 737.
[2] M. Grätzel, *Nature* **2001**, *414*, 338.
[3] P. Wang, S. M. Zakeeruddin, J. E. Moser, M. K. Nazeeruddin, T. Sekiguchi, M. Grätzel, *Nat. Mater.* **2003**, *2*, 402.
[4] J. H. Wu, Z. Lan, J. M. Lin, M. L. Huang, S. C. Hao, T. Sato, S. Yin, *Adv. Mater.* **2007**, *19*, 4006.
[5] Y. Bai, Y. Cao, J. Zhang, M. Wang, R. Li, P. Wang, S. M. Zakeeruddin, M. Grätzel, *Nat. Mater.* **2008**, *7*, 626.
[6] M. Law, L. E. Greene, J. C. Johnson, R. Saykally, P. D. Yang, *Nat. Mater.* **2005**, *4*, 455.
[7] K. Zhu, N. R. Neale, A. Miedaner, A. J. Frank, *Nano Lett.* **2007**, *7*, 69.
[8] K. Zhu, T. B. Vinzant, N. R. Neale, A. J. Frank, *Nano Lett.* **2007**, *7*, 3739.
[9] T. W. Hamann, A. B. F. Martinson, J. W. Elam, M. J. Pellin, J. T. Hupp, *Adv. Mater.* **2008**, *20*, 1560.
[10] a) W. Chen, H. F. Zhang, I. M. Hsing, S. H. Yang, *Electrochem. Commun.* **2009**, *11*, 1057.
[11] Y. C. Qiu, W. Chen, S. H. Yang, *J. Mater. Chem.* **2010**, *20*, 1001.
[12] W. Chen, Y. C. Qiu, Y. C. Zhong, K. S. Wong, S. H. Yang, *J. Phys. Chem. A* **2010**, *114*, 3127.

 © 2010 Wiley-VCH Verlag GmbH & Co. KGaA, Weinheim

[13] Q. F. Zhang, C. S. Dandeneau, X. Zhou, G. Z. Cao, *Adv. Mater.* **2009**, *21*, 4087.
[14] V. E. Ferry, L. A. Sweatlock, D. Pacifici, H. A. Atwater, *Nano Lett.* **2008**, *8*, 4391.
[15] J. Q. Xi, M. F. Schubert, J. K. Kim, E. F. Schubert, M. Chen, S.-Y. Lin, W. Liu, J. A. Smart, *Nat. Photonics* **2007**, *1*, 176.
[16] Q. F. Zhang, T. P. Chou, B. Russo, S. A. Jenekhe, G. Z. Cao, *Angew. Chem.* **2008**, *120*, 2436; *Angew. Chem. Int. Ed.* **2008**, *47*, 2402.
[17] D. H. Chen, F. Z. Huang, Y. B. Cheng, R. A. Caruso, *Adv. Mater.* **2009**, *21*, 2206.
[18] T. P. Chou, Q. F. Zhang, G. E. Fryxell and G. Z. Cao, *Adv. Mater.* **2007**, *19*, 2588.
[19] Y. J. Kim, M. H. Lee, H. J. Kim, G. Lim, Y. S. Choi, N.-G. Park, K. Kim, W. I. Lee, *Adv. Mater.* **2009**, *21*, 3668.
[20] S. Colodrero, A. Mihi, L. Häggman, M. Ocaña, G. Boschloo, A. Hagfeldt, H. Míguez, *Adv. Mater.* **2009**, *21*, 764.
[21] H. J. Koo, Y. J. Kim, Y. H. Lee, W. I. Lee, K. Kim, N. G. Park, *Adv. Mater.* **2008**, *20*, 195.
[22] S. Hore, P. Nitz, C. Vetter, C. Prahl, M. Niggemann, R. Kern, *Chem. Commun.* **2005**, 2011.
[23] P. Wang, S. M. Zakeeruddin, P. Comte, R. Charvet, R. Humphrey-Baker, M. Grätzel, *J. Phys. Chem. B.* **2003**, *107*, 14336.
[24] X. J. Feng, K. Shankar, O. K. Varghese, M. Paulose, T. J. Latempa, C. A. Grimes, *Nano Lett.* **2008**, *8*, 3781.
[25] Y. Diamant, S. Chappel, S. G. Chen, O. Melamed, A. Zaban, *Coord. Chem. Rev.* **2004**, *248*, 1271.
[26] Y. Diamant, S. G. Chen, O. Melamed, A. Zaban, *J. Phys. Chem. B* **2003**, *107*, 1977.
[27] C. M. Liu, S. H. Yang, *Acs Nano* **2009**, *3*, 1025.
[28] A. Chemseddine, T. Moritz, *Eur. J. Inorg. Chem.* **1999**, 235.
[29] G. K. Mor, K. Shankar, M. Paulose, O. K. Varghese, C. A. Grimes, *Nano Lett.* **2006**, *6*, 215.
[30] L. Dloczik, O. Ileperuma, I. Lauermann, L. M. Peter, E. A. Ponomarev, G. Redmond, N. J. Shaw and I. Uhlendorf, *J. Phys. Chem. B* **1997**, *101*, 10281.
[31] T. Oekermann, D. Zhang, T. Yoshida, H. Minoura, *J. Phys. Chem. B* **2004**, *108*, 2227.
[32] J. F. Qian, P. Liu, Y. Xiao, Y. Jiang, Y. L. Cao, X. P. Ai, H. X. Yang, *Adv. Mater.* **2009**, *21*, 3663.

 © 2010 Wiley-VCH Verlag GmbH & Co. KGaA, Weinheim